Frequency shifts in a local oscillator model for the generation of spontaneous otoacoustic emissions by the lizard ear

Wit, Hero; Bell, Andrew

Published in:
Audiology and Neuro-Otology

DOI:
10.1159/000528024

Publication date:
2023

Audiology and Neurotology

Research Article

Audiol Neurotol 2023;28:183–193
DOI: 10.1159/000528024

Received: June 30, 2022
Accepted: November 7, 2022
Published online: January 10, 2023

Frequency Shifts in a Local Oscillator Model for the Generation of Spontaneous Otoacoustic Emissions by the Lizard Ear

Hero P. Wit[a, b] Andrew Bell[c]

[a]Department of Otorhinolaryngology/Head and Neck Surgery, University Medical Center Groningen, University of Groningen, Groningen, The Netherlands; [b]Graduate School of Medical Sciences, Research School of Behavioural and Cognitive Neurosciences, University of Groningen, Groningen, The Netherlands; [c]John Curtin School of Medical Research, The Australian National University, Canberra, ACT, Australia

Keywords
Inner ear · Hair cells · Basilar papilla · Coupled oscillators · Self-sustaining oscillation · Frequency plateaus

Abstract
Introduction: In order to understand human hearing, it helps to understand how the ears of lower vertebrates, like, for instance, lizards, function. A key feature in common is that the ears of both humans and lizards emit faint, pure tones known as spontaneous otoacoustic emissions (SOAEs). More than four decades after their discovery, the mechanism underlying these emissions is still imperfectly understood, although it is known that they are important for improving the sensitivity and sharpness of hearing. In both humans and lizards, the frequencies of SOAEs change by a few percent when static pressure is applied to the tympanic membrane. For the human ear, this observation is normally explained by a so-called global oscillator model (such as with Shera's coherent reflection model), in which the emissions result from standing waves, and external pressure changes the boundary conditions – the stiffness of the oval and round windows – which then has a global effect on the SOAE frequencies. ***Methods:*** Here we investigate how changing parameters of an earlier developed local oscillator model for the lizard ear can change the frequencies of the SOAEs. A major feature of the model is that each oscillator is coupled only to its immediate neighbours. The oscillators then cluster into groups of identical frequency, and each of these so-called frequency plateaus can be taken to represent an SOAE. ***Results:*** Even though the natural (unperturbed) frequencies of all the oscillators remain fixed, here we find for several model parameters that by slightly changing their value the frequency plateaus – the SOAEs – shift by a few percent. Plots of how these changes alter SOAE frequencies are given, and their magnitude corresponds well with observations of SOAE changes in lizards. ***Discussion:*** Investigation of the influence of the change of parameters in an earlier developed local oscillator model for the lizard ear shows that a local oscillator model can explain small SOAE frequency changes as well as a global oscillator model.

Karger@karger.com
www.karger.com/aud

Correspondence to:
Hero P. Wit, hero.wit@ziggo.nl

Introduction

Otoacoustic emissions (OAEs) are sounds emitted by the ear. They were discovered by Kemp [1976, 1978]. Among the several classes of OAEs [Probst et al., 1991], click-evoked and distortion-product OAEs have become an integral part of clinical tests of human hearing.

A special class of OAEs are spontaneous otoacoustic emissions (SOAEs), being narrow-band sounds emitted by an ear in the absence of any acoustic stimulation. SOAEs evidently reflect some internal active process that improves the ear's sensitivity and selectivity. They were predicted theoretically by Gold [1948] based on a "regenerative" model for signal detection.

Nevertheless, despite intensive research into their behaviour, the basic mechanism producing OAEs has proved elusive, and there is still much controversy in the field. In attempting to resolve the issue, there has been a longstanding interest in the hearing of lizards and other reptiles because their ears are simpler than those of mammals [Manley, 1997]. At the same time, both classes of animal share a number of features, most notably the generation of SOAEs, and the general hope is that understanding the lizard ear will prove helpful in understanding human hearing.

In general, there have been two basic approaches to modelling SOAEs, both of which attempt to mimic the production of narrow-band sound energy by incorporating active oscillators. One approach is based on a set of appropriately tuned "local oscillators," which represent, effectively in a one-to-one arrangement, the ear's internal resonant elements. The elements are usually considered to have some degree of nearest-neighbour coupling, and the coupling causes the oscillators to cluster into multiple frequency plateaus, in which each cluster represents an SOAE.

The other approach is the "global oscillator" model [Shera, 2003, 2021, 2022] in which a key role is played by the amplification of standing waves created by multiple internal reflection of waves travelling backwards and forwards along the basilar membrane [Shera and Cooper, 2013, Fig. 2; Shera, 2015, Fig. 2], so that the oscillations which emerge are a collective property of the whole system. This global oscillator model has been extensively used in understanding human SOAEs, and, although commonly accepted, is not entirely free from controversy [Siegel, 2022].

The local oscillator approach is well suited to modelling the behaviour of the lizard ear. First developed by Vilfan and Duke [2008], an SOAE signal is taken to be the sum of the displacements of oscillators arranged in a one-dimensional array extending from low frequencies at one end to high frequencies at the other, with each oscillator having only nearest-neighbour coupling. Individual SOAE peaks in the spectrum of sound picked up by a microphone next to the lizard ear are then understood as the synchronisation of groups of oscillators to a single frequency, reflecting the natural tendency of all coupled oscillators to cluster into discrete frequency plateaus [Ermentrout and Kopell, 1984]. A similar approach was taken in the model of Gelfand et al. [2010], and the same model was also used by Wit et al. [2012, 2020] to give insight into several characteristics of otoacoustic emissions from lizard ears.

Not included in the foregoing local oscillator models, however, is a treatment of how the sum of the individual oscillations is transmitted to the tympanic membrane, and it therefore overlooks the possibility that this transmission process might in some way change the emitted signal. Bergevin and Shera [2010] did develop a model of the lizard ear which included coupling to the middle ear and thereby to the external acoustic environment, but it described only stimulus-frequency otoacoustic emissions, and hair bundles in the model were represented by damped harmonic oscillators. Since the oscillators were passive, the model was unable to describe the generation and emission of spontaneous otoacoustic emissions. For additional detail, see the overview of OAE modelling by Bergevin et al. [2017].

Recently, Wit and Bell [2022] sought to overcome this limitation by representing each of the hair bundles as an active oscillator and allowing the system, through clustering, to generate groups of self-sustained oscillations [Camalet et al., 2000]. Like the earlier work of Wit et al. [2020], the work used the Vilfan and Duke formalism which allowed the coupling parameters to be systematically varied, and the model was also elaborated to include the middle ear as a separate passive oscillator, permitting spontaneous activity of the hair bundles to be conveyed to the eardrum.

SOAEs are very stable over time (daily and monthly cycles show frequency shifts of less than 1% in humans [Bell, 1992]). Notwithstanding, human SOAE frequencies can be changed by a few percent in several experimental ways [De Kleine et al., 2022, Fig. 5]. Many of these are based on changing the impedance of the middle ear, which then affects the boundary conditions for the inner ear, and in this way the global oscillator model can straightforwardly explain shifts in SOAE frequency [Shera, 2022]. The present paper explores frequency shifts

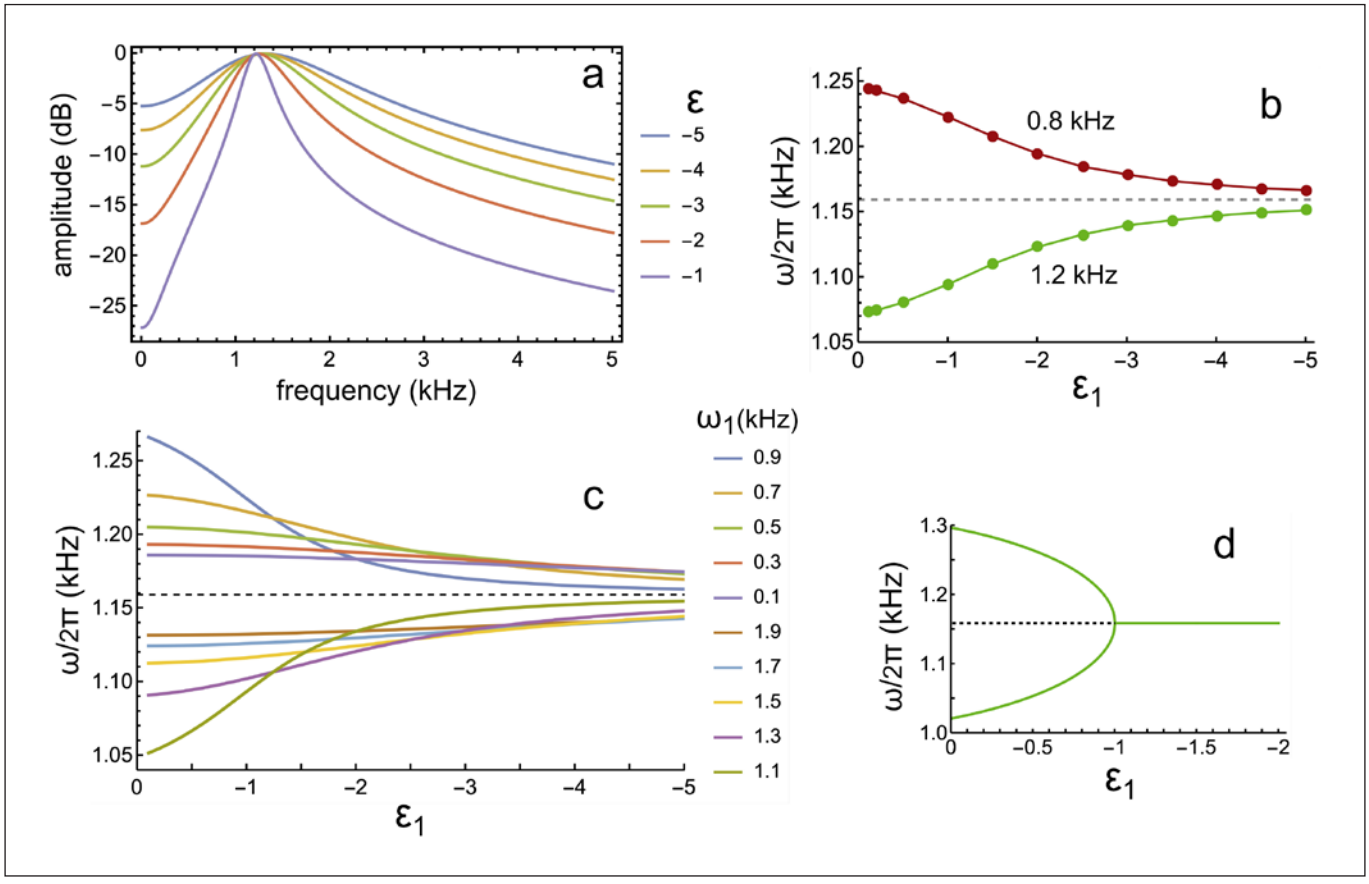

Fig. 1. a Normalised amplitude spectra for the real value of the solution of $\dot{z} = (2\pi i + \epsilon)z - |z|^2 z$, for 5 values of damping parameter ϵ. **b** Common oscillation frequency for the two oscillators, when coupled, calculated with equations (1) for 12 values of ϵ_1, 2 values of the natural frequency of oscillator 1 (0.8 and 1.2 kHz), and a natural frequency of 1 kHz for oscillator 2. **c** Common oscillation frequency for the two oscillators as a function of ϵ_1, calculated with equations (4) for 10 values of the natural frequency of oscillator 1 and a natural frequency of 1 kHz for oscillator 2. **d** Common oscillation frequency for the two oscillators as a function of ϵ_1, if the two oscillators have the same natural frequency of 1 kHz.

in a local oscillator model of the lizard ear and finds that this model can explain observed shifts of SOAE frequency as effectively as the global oscillator model.

Two Oscillators

We start with one active oscillator which drives a second (passive) oscillator and investigate how their common oscillation frequency depends on the choice of parameters. The two oscillators obey the following set of differential equations [Vilfan and Duke, 2008]:

$$\begin{aligned}\dot{z}_1 &= (i\omega_1 + \varepsilon_1)z_1 + (d_R + id_I)(z_2 - z_1) - b|z_1|^2 z_1 \\ \dot{z}_2 &= (i\omega_2 + \varepsilon_2)z_2 + (d_R + id_I)(z_1 - z_2) - b|z_2|^2 z_2\end{aligned} \quad (1)$$

with (complex)

$$z = x - \frac{1}{\omega} i\dot{x}$$

and where x and $\dot{x}$ are, respectively, displacement and velocity (as a function of time) of the oscillators.

In equation (1), ω is the natural frequency of the oscillator (the frequency with which it oscillates if there is no coupling); ϵ is a measure of the effective damping, being positive for an active oscillator and negative for a passive (damped) oscillator; d_R and d_I are, respectively, the dissipative (real) and reactive (imaginary) coupling constants; and b describes the intrinsic nonlinearity of the oscillator and controls its amplitude.

Without coupling ($d_R = d_I = 0$) each oscillator obeys the generic equation for a Hopf bifurcation: $\dot{z} = (i\omega + \epsilon)z - b|z|^2 z$. If this (uncoupled) oscillator is passive ($\epsilon < 0$), its amplitude spectrum is wider for larger (absolute) values of ϵ (Fig. 1a). (For convenience, frequencies are expressed in kilohertz and time in milliseconds).

The set of differential equations (1) was solved with procedure *NDSolve* in *Mathematica 12* (https://www.wolfram.com), for the situation of a passive oscillator ($\epsilon_1 < 0$) coupled to an active oscillator ($\epsilon_2 > 0$).

In this situation, the solution of equations (1), sometime after onset, is a stable sinusoid with the same angular frequency ω for the two oscillators: $z_1(t) = r_1 e^{i(\omega t + \phi_1)}$, $z_2(t) = r_2 e^{i(\omega t + \phi_2)}$. The angular frequency ω of the sinusoid was calculated for the following set of parameters: $\epsilon_2 = 1$, $d_R = 0$, $d_I = -1$, $\omega_2 = 2\pi$, $b = 1$, for two values of ω_1 and a range of values of ϵ_1. The result is shown in Figure 1b.

If the solutions $z_1(t) = r_1 e^{i(\omega t + \phi_1)}$, $z_2(t) = r_2 e^{i(\omega t + \phi_2)}$ are substituted in (1), and the real and imaginary parts are separated, the following set of equations is obtained:

$$\begin{aligned}
&\varepsilon_1 + d_R \frac{r_2}{r_1}\cos(\Delta\phi) - d_R - d_I \frac{r_2}{r_1}\sin(\Delta\phi) - b r_1^2 = 0\\
&\varepsilon_2 + d_R \frac{r_1}{r_2}\cos(\Delta\phi) - d_R + d_I \frac{r_1}{r_2}\sin(\Delta\phi) - b r_2^2 = 0\\
&\omega_1 + d_R \frac{r_2}{r_1}\sin(\Delta\phi) + d_I \frac{r_2}{r_1}\cos(\Delta\phi) - d_I - \omega = 0\\
&\omega_2 - d_R \frac{r_1}{r_2}\sin(\Delta\phi) + d_I \frac{r_1}{r_2}\cos(\Delta\phi) - d_I - \omega = 0
\end{aligned} \tag{2}$$

with $\Delta\phi = \phi_2 - \phi_1$.

Or

$$\begin{aligned}
&\varepsilon_1 + d_R \frac{r_2}{r_1}\beta - d_R - d_I \frac{r_2}{r_1}\alpha - b r_1^2 = 0\\
&\varepsilon_2 + d_R \frac{r_1}{r_2}\beta - d_R + d_I \frac{r_1}{r_2}\alpha - b r_2^2 = 0\\
&\omega_1 + d_R \frac{r_2}{r_1}\alpha + d_I \frac{r_2}{r_1}\beta - d_I - \omega = 0\\
&\omega_2 - d_R \frac{r_1}{r_2}\alpha + d_I \frac{r_1}{r_2}\beta - d_I - \omega = 0\\
&\alpha^2 + \beta^2 - 1 = 0
\end{aligned} \tag{3}$$

with $\alpha = \sin(\Delta\phi)$, $\beta = \cos(\Delta\phi)$.

For the same set of parameters for which equations (1) were solved ($\epsilon_2 = 1$, $d_R = 0$, $d_I = -1$, $\omega_2 = 2\pi$, $b = 1$), equations (3) reduce to

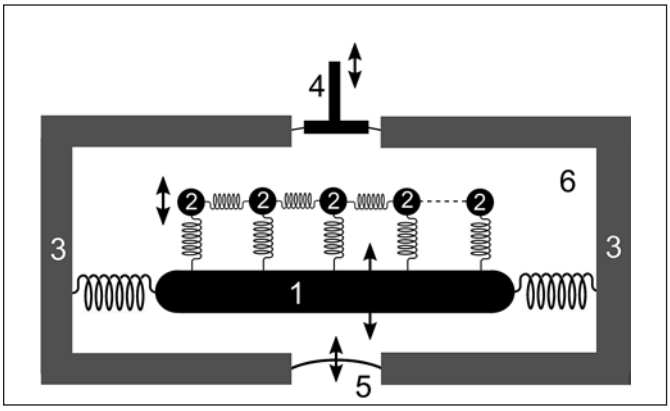

Fig. 2. 1: Solid structure representing the basilar papilla. 2: 200 oscillating hair cell masses. The horizontal springs between the masses represent both dissipative and reactive coupling. 3: Inner ear wall. 4: Stapes. 5: Round window. 6: Inner ear fluid.

$$\begin{aligned}
&\varepsilon_1 + \frac{r_2}{r_1}\alpha - r_1^2 = 0\\
&1 - \frac{r_1}{r_2}\alpha - r_2^2 = 0\\
&\omega_1 - \frac{r_2}{r_1}\beta + 1 - \omega = 0\\
&2\pi - \frac{r_1}{r_2}\beta + 1 - \omega = 0\\
&\alpha^2 + \beta^2 - 1 = 0
\end{aligned} \tag{4}$$

Equations (4) were solved for a range of ω_1 values with *Mathematica 12* procedure *Solve*, for the conditions $r_1 > 0$, $r_2 > 0$, $r_2 > r_1$, to obtain Figure 1c.

Figure 1d is for the situation where the two oscillators have the same natural frequency ($\omega_1 = \omega_2$). In this case there are two regions of solutions of equations (4): one for $\beta = 0$ (with $\alpha = 1$), and the other for $r_1 = r_2 = r$.

For $\beta = 0$, the set of equations (4) has real solutions for $\epsilon_1 < -1$ only. For this condition the frequency of the two oscillators is $(2\pi + 1)/2\pi = 1.159$ kHz.

For $r_1 = r_2 = r$ there is no solution for $\epsilon_1 < -1$. And, if $-1 < \epsilon_1 < 0$, there are two (different) solutions for each value of ϵ_1: one with $\alpha > 0$, $\beta > 0$, $\omega/2\pi < 1.159$ kHz; and the other with $\alpha > 0$, $\beta < 0$, $\Delta\phi > \pi/2$, $\omega/2\pi > 1.159$ kHz.

It can be concluded from Figure 1b, c that the common oscillation frequency of the two coupled oscillators can be changed by several percent by changing the damping and/or the natural frequency of the passive oscillator.

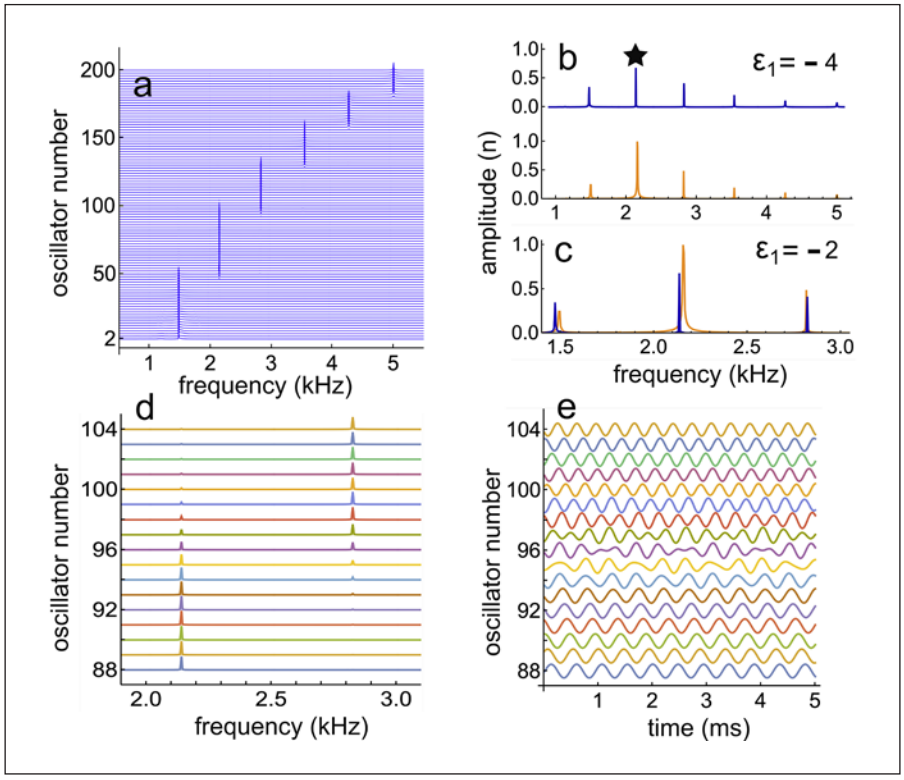

Fig. 3. a Normalised amplitude spectra for $x_j(t)$, for j = 2, 4, 6, …, 200, for a natural frequency of 2.3 kHz and damping parameter of –4 for oscillator 1. **b** Accompanying spectrum for oscillator 1, for 2 values of damping parameter ϵ_1. **c** Zoom view of **b** with spectra overlapped so as to readily reveal shifts. **d** Detail of **a** for oscillators 88–104. Spectral peaks are at 2.13 and 2.83 kHz. **e** A 5 ms time interval for displacements $x_j(t)$, for the same oscillators as in **d**.

Array of 201 Oscillators

How Oscillator Frequencies Depend on the Parameters of the Passive Oscillator

Wit and Bell [2022] used an array of n = 201 coupled oscillators to model the emission of SOAEs from the ear of the lizard. The hair cells in the lizard inner ear were represented in this model by a chain of 200 oscillators. Again, following Vilfan and Duke [2008], the differential equation to be solved for the jth oscillator (j = 2, 3,…, n) is

$$\dot{z}_j = (i\omega_j + \varepsilon_j)z_j + (d_R + id_I)(z_{j-1} - 2z_j + z_{j+1}) - b|z_j|^2 z_j \quad (5)$$

For the first oscillator of the chain of vibrating elements (j = 1), the term ($z_{j-1} - 2z_j + z_{j+1}$) is replaced by ($z_3 - z_2$) and for the last by ($z_{n-1} - z_n$).

Because the inner ear fluid is incompressible, this fluid, the basilar papilla, and the stapes move in phase. They are therefore simply represented by a single oscillator. The displacement as a function of time $Re[z_1(t)]$ of this oscillator then represents the SOAEs measured at the eardrum. The equation for this oscillator is

$$\dot{z}_1 = (i\omega_1 + \varepsilon_1)z_1 - b|z_1|^2 z_1 + \mu\sum_{j=2}^{n} Re[z_j] \quad (6)$$

The last term in equation (6) stands for the total force exerted on the papilla by the vibrating elements. This force is supposed to be proportional to the sum of the displacements $x_j(t)$ of the vibrating elements, with proportionality constant μ. Furthermore, the term $+\mu Re[z_1]$ is added to the right-hand side of equation (5), being the force exerted by the papilla on each vibrating element. Figure 2 is a schematic representation of the model.

The combination of equations (5) and (6) was solved with *Mathematica 12* procedure *NDSolve*, for the following parameter values: ω_j increased exponentially from $\omega_2 = 1 \times 2\pi$ to $\omega_n = 5 \times 2\pi$, b = 0.8, d_R = 0.1, d_I = –1.1, ϵ_j = 0.8 for j = 2, 3, …, n, μ = 0.4, $\omega_1 = 2.3/2\pi$, and ϵ_1 = –2 or –4. Amplitude spectra for the resulting displacements as a function of time, for the subset of oscillators 2–201, are shown in a waterfall plot in Figure 3a. And spectra for the first oscillator are given in Figure 3b, c, Figure 3 shows that the 200 active oscillators, which drive the passive oscillator, have clustered in 6 frequency peaks. Note also that changing the damping ϵ_1 of the passive oscillator results in a small frequency shift for some of the peaks.

The frequency f_s for the peak marked with a star in Figure 3b was calculated for 11 values of the natural frequen-

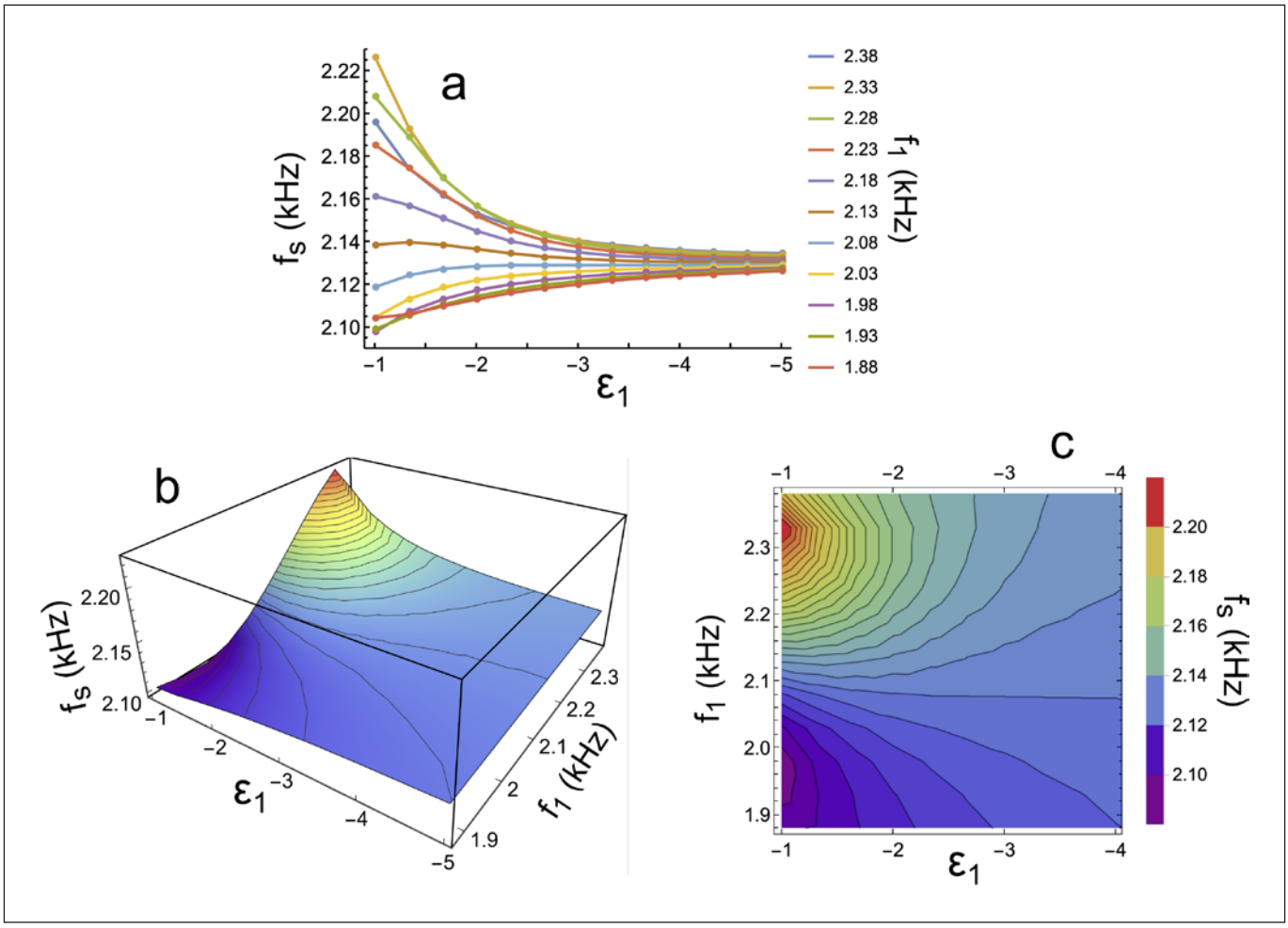

Fig. 4. Frequency f_s of the peak marked with a star in Fig. 3b for 11 values of the natural frequency f_1 of oscillator 1 and 13 values of its damping parameter ϵ_1. **a** In a 2D-plot. **b** In a 3D-plot, smoothed by interpolation. **c** For 10 values of ϵ_1 in a contour plot, also smoothed.

cy f_1 of oscillator 1 and 13 values of its damping parameter ϵ_1. The result is shown in Figure 4.

It can be concluded from Figure 4 that the frequency of the peak marked with a star in Figure 3b, representing an SOAE, can be changed by about 100 Hz (5%) by changing the damping and/or the natural frequency of the passive oscillator (the basilar papilla in Fig. 2).

How the Clustering Frequencies of the Active Oscillators Depend on Their Parameters

Calculations with the combination of equations (5) and (6) were repeated for the following "standard" set of parameters: ω_j increased exponentially from $\omega_2 = 1 \times 2\pi$ to $\omega_n = 5 \times 2\pi$, $b = 0.8$, $d_R = 0.1$, $d_I = -1.1$, $\epsilon_j = 0.8$ for $j = 2, 3, \ldots, n$, $\mu = 0.4$, $\omega_1 = 2.3 \times 2\pi$, and $\epsilon_1 = -4$. In addition, it was done for two other values of one of the parameters. Results are given as amplitude spectra in Figure 5a for three values of reactive coupling parameter d_I and in Figure 5b for three values of dissipative coupling parameter d_R.

Figure 6 is the same as Figure 5, for three values of two other parameters. To obtain Figures 6a, b, amplitude spectra were calculated for 3 values of the damping parameter ϵ, for all oscillators except oscillator 1. While for Figures 6c, d, the natural frequencies ω_j were multiplied with 0.98, 1, or 1.02 (for all j except $j = 1$). This multiplication factor (χ_ω) changes the natural frequency of the oscillators up or down by 2 percent (and provides a reference point for other shifts induced by altering other parameters away from their "standard" values).

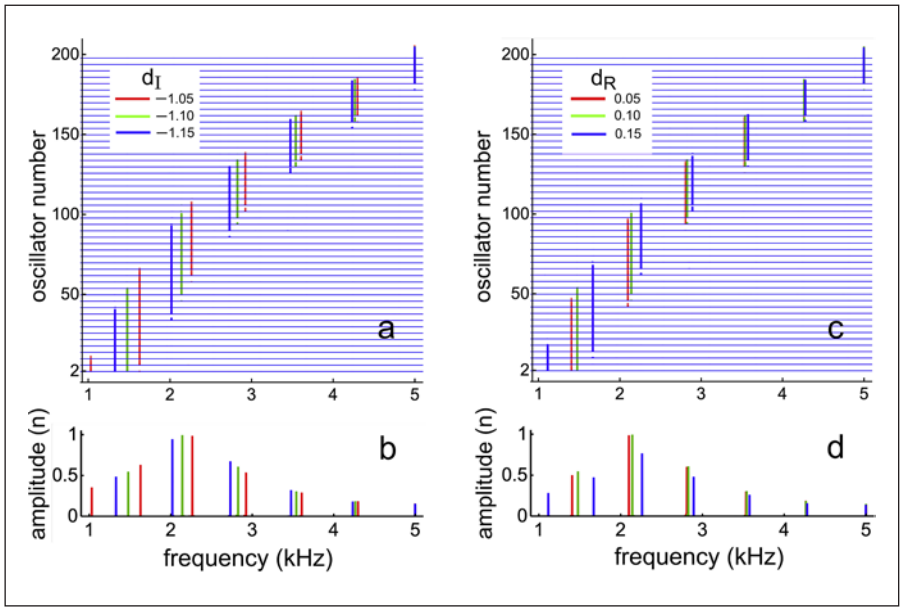

Fig. 5. a Amplitude spectra for $x_j(t)$, for oscillator numbers $j = 2, 6, 10, \ldots, 198$ and for 3 values of reactive coupling parameter d_I. **b** Amplitude spectra for oscillator 1, for the same set of parameters as for **a**. **c**, **d** Same as **a** and **b**, for 3 values of dissipative coupling parameter d_R.

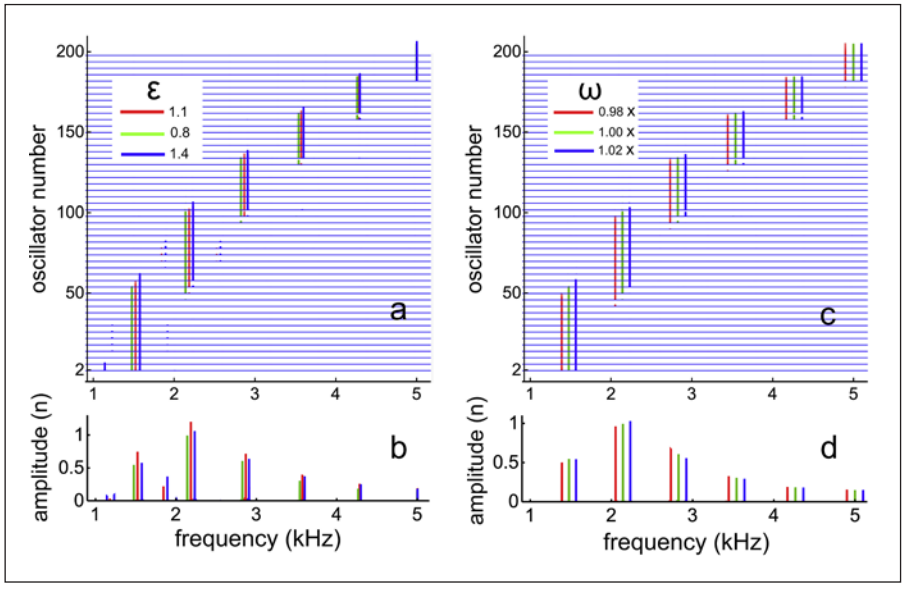

Fig. 6. a Amplitude spectra for $x_j(t)$, for oscillator numbers $j = 2, 6, 10, \ldots, 198$ and for 3 values of damping parameter ϵ. **b** Amplitude spectra for oscillator 1, for the same set of parameters as for **a**. **c**, **d** Same as **a** and **b**, for 3 values of the frequency multiplication factor χ_ω.

The calculations to obtain Figures 5 and 6 were repeated for 13 values of d_I, d_R, ϵ_j, or the multiplication factor χ_ω of ω_j. The results are given in Figure 7. Frequency f_s in this figure is the frequency of the peak around 2.13 kHz in the spectra in Figures 5 and 6. (It is also the spectral peak marked with a star in Fig. 3b). The vertical dashed lines in Figure 7 mark the "standard" values for d_I, d_R, ϵ_j, and χ_ω, being −1.1, 0.1, 0.8, and 1, respectively.

To obtain a 1% change of f_s, starting at the value marked with the horizontal dashed line in Figure 7, the values d_I, d_R, ϵ_j, or χ_ω need to be changed by 0.8, 13, 18, or 0.5%, respectively.

Discussion

This paper has used numerical modelling to investigate what we claim to be, in essence, a simple system. Its mathematical flavour, however, has meant that much of the methods and results may not be readily accessible to those with a clinical background. The following discussion is designed to highlight aspects of the work that relate to how real ears function, most directly to the lizard ear but also perhaps the human ear as well.

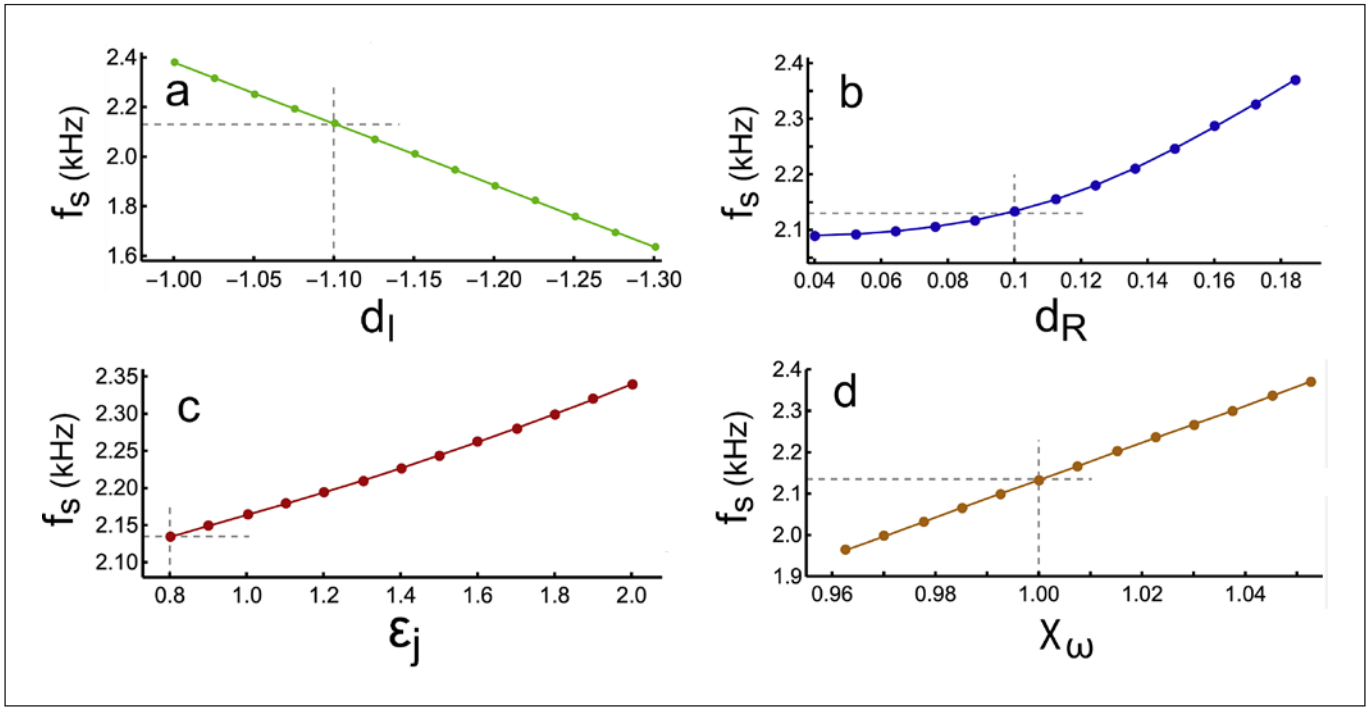

Fig. 7. a Frequency f_s of the dominant spectral peak in Figure 5b for 13 values of d_I. **b** For 13 values of d_R. **c** Frequency f_s of the dominant peak in Figure 6b for 13 values of ϵ_j. **d** For 13 values of χ_ω. The vertical dashed lines mark the "standard" position of the parameters.

Model Schematic

Our model of the lizard ear (Fig. 2) assumes that all the active oscillators, representing hair cells, sit on top of a passive substrate representing the basilar papilla, which in this work we have labelled as oscillator 1. This oscillator is surrounded by fluid, and this means that any vibration imparted to the substrate by the hair cells will in turn be communicated to the eardrum, and thence to the outside world, where it can be picked up as an SOAE. It is worth noting that the reverse of this process is the way by which outside sound is communicated to the hair cells, so the system is equivalent to a resonant detector, such as the vibrating reed frequency metre [Bell and Wit, 2015]. An earlier – somewhat simpler – version of the model was used to investigate another type of OAEs: the stimulus frequency otoacoustic emission (SFOAE) [Wit et al., 2012].

Clustering of Oscillators

Our numerical simulations have confirmed a well-known result: that a linear, graded array of coupled oscillators will cluster into a number of discrete frequency plateaus. Within a cluster, all the oscillators are vibrating at the same frequency, and it has been suggested in several earlier papers [Vilfan and Duke, 2008; Gelfand et al., 2010; Wit et al., 2012, 2020; Wit and Bell, 2022] that each cluster could well represent an SOAE from the ear of a lizard.

As can be seen in Figure 3a, and in detail in Figure 3d, not all oscillators in our model exhibit a single spectral peak: two peaks exist in the transition region between two clustering frequencies. The lower-frequency spectral peak grows smaller with increasing oscillator number, while the higher-frequency peak grows larger. Examination of Figure 3e reveals this behaviour in the time domain: the displacement $x_j(t)$ of oscillator 96, for example, is the sum of two sine waves of 2.13 and 2.83 kHz; at the same time, the behaviour of oscillators 88 and 104 (away from the transition region) are single sines of either 2.13 or 2.83 kHz.

Vilfan and Duke [2008] displayed their results in a slightly different way. To make frequency plateaus apparent, they calculated the average frequency of each of the oscillators, thus showing that each oscillator possessed only a single frequency. Following the same approach, we calculated the average frequencies of the oscillators by

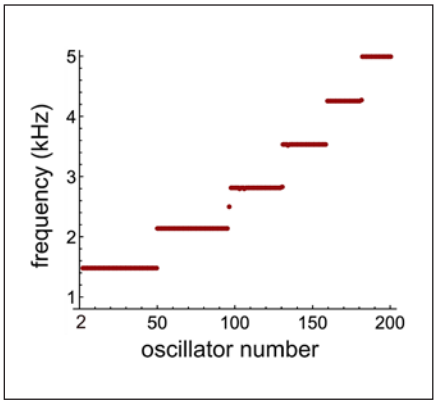

Fig. 8. Another way of demonstrating the appearance of frequency plateaus. Here the average frequencies of oscillators 2–200 are shown for the same parameters as in Figure 3a.

counting the number of 2π phase jumps (periods) over 50 ms. The result is given in Figure 8. Different approaches to calculating the frequency of oscillators clustering within a frequency plateau are treated in more detail in Moretto Sørensen et al. [2019].

How the Oscillators Are Coupled

In the present model, an important property is that the oscillators are coupled to their nearest neighbours only (one on either side), as in the models for the lizard ear by Vilfan and Duke [2008] and Gelfand et al. [2010]. This simple arrangement has also been used in the models of Wit et al. [2012] and, more recently, in the model of Moretto Sørensen et al. [2019].

Because it is generally accepted that hair cells (or their bundles) are the oscillators in a real ear, Faber and Bozovic [2021] recently explored synchronisation of coupled hair cells in an in vitro preparation of the bullfrog sacculus to lend "support to the theory that SOAEs may be generated by frequency clustering of actively oscillating hair bundles." Similar to our approach, Faber and Bozovic describe the behaviour of the 10 oscillators in their model using the generic equation for a Hopf bifurcation, with the limit cycle frequencies of the oscillators spanning a range from 1 to 4.5 kHz. But in contrast to our approach, the oscillators are not just coupled to their nearest neighbours, but each oscillator (hair bundle) is coupled to an overlying membrane, with coupling strength k_j for the jth oscillator; the coupling term is $k_j(\bar{z} - z_j)$, with

$$\bar{z} = \frac{1}{N}\sum_{j=1}^{N} k_j z_j$$

for N oscillators. If each k_j value is randomly selected from a uniform distribution spanning 0.2–3.0, and supposing that "it is unlikely that the level of attachment to the membrane is identical for all oscillators," some oscillators synchronise while others oscillate incoherently. For this choice of parameters, the model exhibits a complex chimera state, supposed to be "a favourable state for reliable signal detection."

More like the approach used here, Faber and Bozovic also examined the situation in which all k_j were given the same value, so that the oscillators formed discrete clusters of defined frequency (provided the other parameters are given appropriate values). However, in this case, the authors thought that such an arrangement was "unfavorable for detecting frequencies that span several octaves." We leave the matter for further investigation but underline the simplicity of having a uniform coupling parameter along the length of the papilla which is systematically changed due to imposed pressure.

To describe the statistics of (human) SOAEs, the one-dimensional cochlear model of Fruth et al. [2014] employs two types of coupling: longitudinal (for example, by the tectorial membrane) and hydrodynamic, via the fluid. In this case, the parameter $\varepsilon(x)$ that controls the state of the oscillator at position x in the array is chosen to be around zero (it is a spatial version of an Ornstein–Uhlenbeck process, illustrated in Fig. 2b of Fruth et al. [2014] and Fig. 10 of Wit et al. [2020]). The result of this arrangement is that groups of oscillators are randomly active or passive along the cochlear partition. Where the oscillators are active, they produce emissions and tend to synchronise, in the words of Fruth et al. [2014], through "a mixture of hydrodynamic, elastic, and viscous interactions." In this way, coupling of the active oscillators also "depends on global features of the system," and this is basically the same approach as used by Faber and Bozovic [2021] where all the oscillators were coupled to the same overlying membrane.

A feature of the model by Faber and Bozovic [2021] is that it is generic, in the sense that it assumes nothing about the spatial arrangement of the oscillators. This is in contrast with, for instance, the model by Dierkes et al. [2008], where the hair bundles are arranged in a regular two-dimensional pattern and are elastically coupled to their neighbours via an overlying membrane.

Frequency Shifts

The most important results of the present work are shown in Figures 3c, 4, 5 b, d, 6b, d, and 7. These figures

show that the peaks – representing an SOAE – in the spectra for oscillator 1 (the papilla) shift by a few percent when a variety of model parameters are systematically changed. The shifts can be either upward or downward in frequency.

As far as we know, there is only one report of experimentally observed frequency shifts of lizard SOAEs. Van Dijk and Manley [2013] found that small changes of air pressure against the eardrum of five lizard species led to changes in frequency of otoacoustic emissions. These changes, both up and down, and for both increases and decreases in pressure, had a magnitude of a few percent (Van Dijk and Manley [2013], Fig. 2). These authors explained the observed changes as an alteration of the impedance that loads the inner ear emission generators. This explanation in congruent with the results of our modelling as shown in Figures 1 and 4 (although we use slightly different words to describe what is going on). However, in both accounts, a change in the parameters for the passive oscillator – which is driven by 1 (Fig. 1) or 200 (Fig. 4) active oscillators – results in a change in frequency of a few percent. The magnitude of the change depends on the size of the parameter change.

De Kleine et al. [2022] recently gave a summary of the experimental procedures that can cause a change in the frequency of human SOAEs (their Fig. 5). Specifically, they were changes in ear canal pressure, body posture, and middle ear muscle tension. Contralateral acoustic stimulation and stimulation with low-frequency sound also induce shifts. To this list, they add the finding that carbamazepine (a drug prescribed for epilepsy and neuropathic pain) causes human SOAEs to shift upward in frequency by about 3%. In a complementary way, it has long been known that human SOAEs show a diurnal and monthly cycle in their frequencies [Wit, 1985; Bell, 1992].

The fact that SOAE frequencies can be changed in several very different ways (including, for the frog, by injection of direct current to the ear [Wit et al.,1989]), strengthens the idea that no one single mechanism underlies the observed changes. Not only can SOAE frequencies be changed by alterations in middle ear-inner ear transmission, but, evidently, also by changes in inner ear parameters, as modelled here. This implies that, in terms of SOAE frequency changes, no definite conclusion can be drawn in favour of a global oscillator model [Shera, 2003, 2021, 2022] or a local oscillator model. Both are able to produce small frequency shifts given appropriate adjustment of parameters.

Concluding Remarks

Almost 40 years ago, it was shown that the waveform of a human SOAE has the characteristics of an (active) oscillator, driven by noise [Bialek and Wit, 1984]. Since then, various models have been put forward to try to explain the features of SOAEs from the ears of different species. All these models have in common that they incorporate energy-supplying structures (the "cochlear amplifier" [Davis, 1983]), most probably being hair cells and/or their hair bundles [Martin and Hudspeth, 1999; Faber and Bosovic, 2021]. The difference between the models lies in the way along which the energy reaches the tympanic membrane to be emitted as an SOAE.

Statement of Ethics

An ethics statement was not required for this type of study as no human or animal subjects or material was used.

Conflict of Interest Statement

The authors have no conflicts of interest to declare.

Funding Sources

The authors received no financial support for the research and authorship of this article.

Author Contributions

Hero Wit developed the model, did the calculations, and drafted the first version of the manuscript. Andrew Bell and Hero Wit jointly wrote the final version of the manuscript. Both authors approved the final version of the manuscript.

Data Availability Statement

All data generated during this study are included in this article. Further enquiries should be directed to the corresponding author.

References

Bell A. Circadian and menstrual rhythms in frequency variations of spontaneous otoacoustic emissions from human ears. Hearing Res. 1992;58(1):91–100.

Bell A, Wit HP. The vibrating reed frequency meter: digital investigation of an early cochlear model. PeerJ. 2015 Oct 13;3:3e1333.

Bergevin C, Shera CA. Coherent reflection without traveling waves: on the origin of long-latency otoacoustic emissions in lizards. J Acoust Soc Am. 2010;127(4):2398–409.

Bergevin C, Verhulst S, Van Dijk P. Remote sensing the cochlea: otoacoustics. In: Manley GA, Gummer AW, Popper AN, Fay RR, editors. Understanding the cochlea. Springer handbook of auditory research. New York, NY: Springer; 2017. 62.

Bialek W, Wit HP. Quantum limits to oscillator stability: theory and experiments on acoustic emissions from the human ear. Phys Lett A. 1984;104(3):173–8.

Camalet S, Duke T, Jülicher F, Prost J. Auditory sensitivity provided by self-tuned critical oscillations of hair cells. Proc Natl Acad Sci U S A. 2000;97(7):3183–8.

Davis H. An active process in cochlear mechanics. Hearing Res. 1983;9(1):79–90.

De Kleine E, Maat B, Metzemaekers JD, Van Dijk P. Carbamazepine induces upward frequency shifts of spontaneous otoacoustic emissions. Hear Res. 2022;420:108492.

Dierkes K, Lindner B, Jülicher F. Enhancement of sensitivity gain and frequency tuning by coupling of active hair bundles. Proc Natl Acad Sci U S A. 2008;105(48):18669–74.

Ermentrout GB, Kopell N. Frequency plateaus in a chain of weakly coupled oscillators, I. SIAM J Math Anal. 1984;15(2):215–37.

Faber J, Bozovic D. Chimera states and frequency clustering in systems of coupled inner-ear hair cells. Chaos. 2021;31(7):073142.

Fruth F, Jülicher F, Lindner B. An active oscillator model describes the statistics of spontaneous otoacoustic emissions. Biophysical J. 2014;107(4):815–24.

Gelfand M, Piro O, Magnasco MO, Hudspeth AJ. Interactions between hair cells shape spontaneous otoacoustic emissions in a model of the tokay gecko's cochlea. PLoS One. 2010;5(6):e11116.

Kemp DT. Active resonance systems in audition. Abstracts: 13th International Congress of Audiology; 1976. p. 64–5.

Gold T. Hearing II. The physical basis of the action of the cochlea. Proc R Soc B. 1948;135(881):492–8.

Kemp DT. Stimulated acoustic emissions from within the human auditory system. J Acoust Soc Am. 1978;64(5):1386–91.

Manley GA. Diversity in hearing-organ structure and the characteristics of spontaneous otoacoustic emissions in lizards. In: Lewis ER, Long GR, Lyon RF, Narins PM, Steele CR, editors. Diversity in Auditory Mechanics. Singapore: World Scient Publ; 1997. p. 32–8.

Martin P, Hudspeth AJ. Active hair-bundle movements can amplify a hair cell's response to oscillatory mechanical stimuli. Proc Natl Acad Sci U S A. 1999;96(25):14306–11.

Moretto Sørensen L, Bysted PL, Epp B. Clustering in an array of nonlinear and active oscillators as a model of spontaneous otoacoustic emissions. Proceedings of the ICA 2019 and EAA Euregio. 2019. https://pub.dega-akustik.de/ICA2019/data/articles/000796.pdf

Probst R, Lonsbury-Martin BL, Martin GK. A review of otoacoustic emissions. J Acoust Soc Am. 1991;89(5):2027–67.

Shera CA. Mammalian spontaneous otoacoustic emissions are amplitude-stabilized cochlear standing waves. J Acoust Soc Am. 2003;114(1):244–62.

Shera CA, Cooper NP. Basilar-membrane interference patterns from multiple internal reflection of cochlear traveling waves. J Acoust Soc Am. 2013;133(4):2224–39.

Shera CA. Iterated intracochlear reflection shapes the envelopes of basilar-membrane click responses. J Acoust Soc Am. 2015;138(6):3717–22.

Shera CA. Whistling while it works: spontaneous otoacoustic emissions and the cochlear amplifier. JARO. 2022;23(1):17–25.

Siegel J. Wide bandwidth of ear-canal otoacoustic emission signals supports fast reverse propagation from organ of Corti through fluid pressure. In: Abstracts 45th Annual Midwinter Meeting Association for Research in Otolaryngology. ARO MidWinter Meeting Archives; 2022. p. 128–9.

Van Dijk P, Manley GA. The effects of air pressure on spontaneous otoacoustic emissions of lizards. JARO. 2013;14(3):309–19.

Vilfan A, Duke T. Frequency clustering in spontaneous otoacoustic emissions from a lizard's ear. Biophysical J. 2008;95(10):4622–30.

Wit HP, Bell A. From hair bundle to eardrum: an extended model for the generation of spontaneous otoacoustic emissions by the lizard ear. J Hear Sci. 2022;12(2):9–19.

Wit HP, Manley GA, Van Dijk P. Modeling the characteristics of spontaneous otoacoustic emissions in lizards. Hearing Res. 2020;385:107840.

Wit HP, Van Dijk P, Manley GA. A model for the relation between stimulus frequency and spontaneous otoacoustic emissions in lizard papillae. J Acoust Soc Am. 2012;132(5):3273–9.

Wit HP, Van Dijk P, Segenhout JM. DC injection alters spontaneous otoacoustic emission frequency in the frog. Hearing Res. 1989;41(2-3):199–204.

Wit HP. Diurnal cycle for spontaneous otoacoustic emission frequency. Hearing Res. 1985;18(2):197–9.